AGU PUBLICATIONS

JGR

Journal of Geophysical Research: Planets

RESEARCH ARTICLE
10.1002/2013JE004570

**Key Points:**
- Three-dimensional structure would not affect attempts to detect a liquid ocean
- Three-dimensional structure would not affect attempts to determine the mean shell thickness
- Presence of 3-D structure could be inferred from nondegree-2 tidal response

**Correspondence to:**
G. A,
geruo.a@colorado.edu

**Citation:**
A, G., J. Wahr, and S. Zhong (2014), The effects of laterally varying icy shell structure on the tidal response of Ganymede and Europa, *J. Geophys. Res. Planets*, *119*, 659–678, doi:10.1002/2013JE004570.

Received 1 NOV 2013
Accepted 10 FEB 2014
Accepted article online 1 MAR 2014
Published online 28 MAR 2014

# The effects of laterally varying icy shell structure on the tidal response of Ganymede and Europa

**G. A[1,2], J. Wahr[1,2], and S. Zhong[1]**

[1]Department of Physics, University of Colorado Boulder, Boulder, Colorado, USA, [2]Also at Cooperative Institute for Research in Environmental Sciences, University of Colorado Boulder, Boulder, Colorado, USA

**Abstract** We use a finite-element model to solve for the response of Ganymede and Europa to tidal forcing from Jupiter, using various icy shell models with laterally variable (3-D) structure. In all cases, the shell is assumed to be underlain by a liquid-water ocean. Icy shells with laterally varying thickness are derived from a thermal conduction model. Three-dimensional shear modulus profiles for the shell are built either from a conduction model or, for Europa, by assuming a hemispherical difference in composition. Icy shell structures with a nonglobal ocean are built for Ganymede. Using these shell structures to calculate the tidal response of Ganymede and Europa, we conclude the following: (1) the presence of lateral variations in thickness or in shear modulus would not degrade future attempts to use tidal observations to decide on the existence or absence of a liquid ocean and to determine the mean icy shell thickness. (2) Given accurate enough observations, the presence of lateral variations in thickness or in shear modulus could be determined by searching for nondegree-2 components in the tidal response. (3) In the absence of significant viscous convective flow in the shell, the effects of a laterally varying shear modulus on the tidal response would be smaller than those of a laterally varying shell thickness. (4) If the shell is partially grounded, tidal observations of either gravity or uplift would be able to roughly differentiate regions where the ice is grounded from those where it is floating.

## 1. Introduction

One of the long-sought objectives of an orbiter or flyby mission to one of Jupiter's icy moons has been to use observations of tides on the Moon to help determine the existence of a liquid ocean and characteristics of the overlying icy shell. The radio science component of such a mission could be used to estimate the degree-2 tidal potential Love number $k_2$. And if there is an onboard laser altimeter, it could be used to map out tidal displacements [see, e.g., *Smith et al.*, 2001; *Neumann et al.*, 2001] and to determine the degree-2 radial displacement Love number $h_2$. Knowledge of either of those Love numbers could provide information on the presence of an ocean beneath the icy outer shell [see, e.g., *Yoder and Sjogren*, 1996; *Edwards et al.*, 1996; *Moore and Schubert*, 2000; *Wu et al.*, 2001; *Wahr et al.*, 2006], and the two Love numbers could be combined to place constraints on the thickness of the icy shell [*Wahr et al.*, 2006].

But if a subsurface ocean exists, complications could conceivably arise if the icy outer shell has significant lateral variations in either its thickness or its shear modulus, or if the ocean is not global in extent so that the shell is grounded in places but floating in others. In those cases, the tidal deformation pattern would not be solely represented as the sum of degree-2 harmonics, and so neither the gravity nor the uplift could be completely described by the Love numbers $k_2$ and $h_2$.

In this study, simple but plausible assumptions are used to build various icy shell models with laterally varying (3-D) structures. The 3-D variations in the models are chosen to be large, so that an upper bound estimate of 3-D effects can be investigated. By solving a set of tidal forcing problems using these laterally variable icy shell structures, we examine how those structures might complicate the interpretation of tidal measurements, and we discuss how to extract information regarding the interior structure of Ganymede and Europa from measurements of their tidal response.

Section 2 briefly discusses the numerical model we use to solve the tidal forcing problem. In section 3, we introduce our test structures for Ganymede and Europa's icy outer shells. Icy shell structures with laterally varying shell thickness are derived from a thermal conduction model. Three-dimensional shear modulus profiles of the ice are obtained either from a conduction model or, for Europa, by assuming a compositional


©2014. American Geophysical Union. All Rights Reserved.

**Table 1.** The Spherically Symmetric Satellite Structure Used as the Default Models for Ganymede and Europa[a]

| | Ganymede | Europa |
|---|---|---|
| Radius of the satellite (km) | 2638 | 1565 |
| Radius to the top of the rocky mantle (km) | 1913 | 1265 |
| Radius to the top of the core (km) | 630 | 700 |
| Density of the ice (kg/m$^3$) | 1040 | 1000 |
| Density of the rocky mantle (kg/m$^3$) | 3300 | 5150 |
| Density of the core (kg/m$^3$) | 5147 | 5150 |
| Bulk modulus in the ice (GPa) | 10 | 10 |
| Bulk modulus in the rocky mantle (GPa) | 110 | 120 |
| Shear modulus in the ice (GPa) | 2 | 2 |
| Shear modulus in the rocky mantle (GPa) | 10 | 120 |

[a]Both satellites contain a fluid core, a rocky mantle, and an ice/ocean layer. The density of the ocean is the same as for the ice.

difference between the leading and trailing hemispheres. We also take Ganymede as an example and build test structures for the case of a partially grounded icy shell. Using these shell structures, we compute the tidal response of the icy satellites. The results and their implications are discussed in section 4 and summarized in section 5. We also include an Appendix A to discuss the numerical properties of our finite-element solutions.

## 2. Numerical Model

To solve the tidal forcing problem, we use the finite-element model CitcomSVE that was designed to compute the viscoelastic response of a 3-D compressible Earth to surface loading [*A et al*., 2013]. That same numerical model has been used to address the tidal response of the Earth's Moon with 3-D internal structure [*Zhong et al*., 2012]. CitcomSVE was developed originally for modeling the glacial isostatic adjustment process for an incompressible Earth with 3-D viscoelastic structures [*Zhong et al*., 2003; *Paulson et al*., 2005]. The physical model and the numerical method for tidal deformation applications, and the benchmark results for spherically symmetric models, have been discussed in detail by *A et al*. [2013] and *Zhong et al*. [2012]. For the finite-element grid, we divide each satellite's mantle into 12 caps of approximately equal size, and each cap is further divided into 80 cells in each horizontal direction and 80 cells in the radial direction. So the total number of elements is $12 \times 80 \times 80 \times 80$ [see, e.g., *Zhong et al*., 2008].

The tidal forcing acting on the icy satellites is mainly induced by the gravitational attraction of Jupiter. To first order in the satellite's eccentricity, and assuming the satellite's inclination is 0, the diurnal tidal potential can be written as [see, e.g., *Kaula*, 1964; *Wahr et al*., 2009; *Jara-Orué and Vermeersen*, 2011]

$$V_T(r,\theta,\varphi,t) = A\left(\frac{r}{R}\right)^2 \left[(1-3\cos^2\theta)\cos(nt) + \sin^2\theta[3\cos(nt)\cos(2\varphi) + 4\sin(nt)\sin(2\varphi)]\right] \quad (1)$$

where $A = 3GM\varepsilon R^2/4a^3$. Here $r$, $\theta$, $\varphi$ are the radius, colatitude, and eastward longitude; $M$ is Jupiter's mass; $R$, $a$, and $n$ are the satellite's radius, semimajor axis, and mean motion; and $\varepsilon$ is the orbital eccentricity. Here we do not include the static tidal potential in our calculation, because the entire satellite presumably responds to that static field as an inviscid fluid. The static tidal potential would cause a permanent equatorial bulge fixed to the satellite, but there would be no tidal shear stresses associated with that bulge, since all stresses would have had time to relax. For the diurnal tide, $V_T$ is the sum of spherical harmonics of degree-2 and varies periodically with time at a period of 7.15 days for Ganymede and 3.55 days for Europa. In our numerical model, we assume that the icy satellite deforms elastically in response to the tidal potential. In equation (1), $V_T$ consists of both (2, 0) forcing (the $(1-3\cos^2\theta)$ term) and (2, 2) forcing (the $\sin^2\theta$ term) (we use the notation ($l$, $m$) to represent degree-$l$ and order-$m$ throughout this paper). For simplicity, we include forcing from only the (2, 0) term in our numerical calculations, with the assumption that our conclusions about the general importance of 3-D structure would be the same for (2, 2) forcing.

As input to the numerical model, we build a simplified multilayer satellite structure for both Ganymede and Europa (see Table 1). Both satellites contain an inviscid fluid core, a rocky mantle, an overlying liquid ocean, and an outer icy shell. The structure of the icy satellites' core is not well constrained. For Ganymede, the observed intrinsic magnetic field suggests the existence of a liquid core [*Schubert et al*., 1996], while for Europa, the structure and composition of the core are still largely uncertain [see, e.g., *Schubert et al*., 2009]. However, because the existence of a subsurface liquid ocean dramatically reduces the coupling between the surface and the layers below the ocean, the structural and rheological properties of the core have relatively little effect on the pattern or amplitude of the surface tidal response. In its present form, the 3-D numerical code cannot include an inviscid fluid layer (e.g., a liquid ocean) unless it extends to the center of the satellite. To circumvent this problem, we assume that the rocky mantle, liquid ocean, and icy shell are all Maxwell


©2014. American Geophysical Union. All Rights Reserved.

viscoelastic solids, and we assign a low viscosity ($10^{11}$ Pa s) to the ocean layer and a high viscosity ($10^{20}$ Pa s) to the ice and rocky mantle. We denote the ocean layer's characteristic relaxation time as $\tau_o$. This is determined by the low viscosity in the ocean layer and is orders of magnitude smaller than the relaxation time of the solid layers. We force the system with a tidal potential that is held constant in time and let the system relax viscously. After hundreds of $\tau_o$s, the ocean layer reaches its fluid limit while the ice and rocky mantle still behave elastically (see Appendix A for details).

In general, the presence of a liquid ocean tends to decouple the mantle deformation below the ocean from that above the ocean, and as a result the surface tidal response is largely insensitive to the depth of the ocean. Although it is likely that at least for Ganymede, there is a high-pressure ice layer between the ocean and the rocky mantle [*Anderson et al.*, 1996], in our models (see Table 1), we assume that the ocean extends downward to lie directly on top of the rocky mantle, which leads to a relatively thick ocean for both satellites. This model configuration does not change the tidal response solutions significantly, but it does help increase the convergence speed of the numerical calculation. As shown in Table 1, we use simplified density structures for both satellites. We assume that the density of the ocean is the same as for the ice. And for Europa, we use the same density for the rocky mantle as for the fluid core. These assumptions simplify the density structure and lead to relatively large surface gravity accelerations, but they do not impact our general conclusions regarding the impact of 3-D shell structures. In the following section, we build laterally varying structures for the outer icy shell, which are incorporated into the layered satellite models and are used to obtain the tidal response.

## 3. Outer Icy Shell Models

We consider three possible sources of 3-D structure for the outer icy shell: lateral variations in temperature that lead to variations in shell thickness and shear modulus; hemispherically dependent compositional differences that cause 3-D variations in shear modulus; and a shell that is partially grounded and partially floating. Our models for these types of structures are described in the following three subsections.

### 3.1. Icy Shell Structure From a Conduction Model

The thickness and elastic properties of an icy shell are directly related to its thermal state. The ice thickness could be significantly nonuniform if the temperature distribution of the ice is determined by thermal conduction. In contrast, if the ice is convecting [*Pappalardo et al.*, 1998] or is undergoing significant lateral flow, there should be little lateral variability in shell thickness [see, e.g., *Nimmo and Manga*, 2009]. The lateral variability of elastic properties (e.g., the shear modulus) of the ice also depends on how much lateral variability is present in the temperature field. In this study, one of our primary goals is to determine the maximum plausible effects of laterally varying shell structure on tidal observables. To achieve this end, we assume that thermal conduction is the dominant heat transfer mechanism, and we choose parameters that lead to large lateral variations in the temperature field of the icy shell. Using this temperature field, we build hypothetical shell models where the lateral variations in shell thickness and/or elastic properties are plausible, but large.

#### 3.1.1. Theory and Method

In a conduction model, there are three factors that can influence the lateral variations in temperature: the surface temperature, the tidal dissipation within the icy shell, and the heat flux at the bottom of the shell. The surface temperature of the satellite is determined by the distribution of solar insolation. Its value depends on latitude and is relatively uniform near the equator [*Ojakangas and Stevenson*, 1989; *Nimmo et al.*, 2007]. The spatial pattern of the tidal dissipation is directly related to the degree-2 tidal potential and causes the temperature field to vary with both latitude and longitude. Although the basal heat flux can vary with position as well, that variation is not well constrained. So we assume that the basal heat flux is uniform. In general, large basal heating tends to reduce the mean thickness of the icy shell and to eliminate lateral variations induced by internal heating (i.e., the tidal dissipation). In this study, we choose a value of the basal heat flux that causes the shell thickness to be reasonably small and the lateral variations from the tidal dissipation to be large, which gives more relative lateral variability to the shell structure, especially at low latitudes.

The surface temperature variations are computed based on the theory given in *Ojakangas and Stevenson* [1989, Appendix A]. Tidal dissipation rates are computed using the method given in *Ojakangas and Stevenson*


©2014. American Geophysical Union. All Rights Reserved.

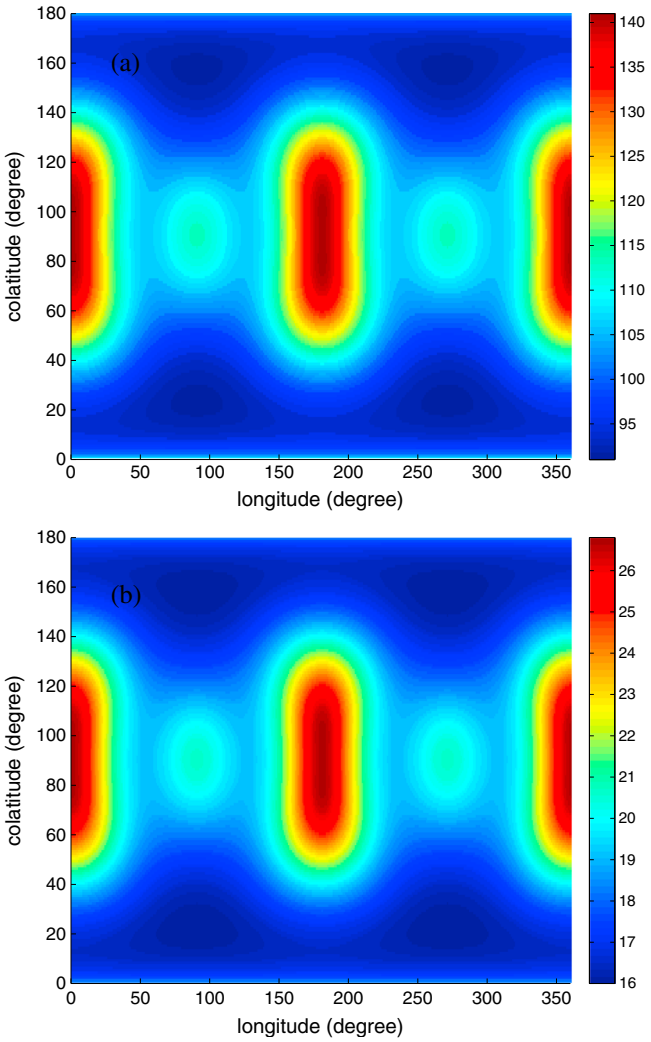


**Figure 1.** The icy shell thickness models: (a) model GA for Ganymede and (b) model EA for Europa. The color bar shows the ice thickness in kilometer.

[1989, Appendix B] and in *Nimmo et al.* [2007]. Following the finite-difference method described in *Nimmo et al.* [2007] and using the parameters and methods described below, we obtain a laterally varying temperature field and the 3-D variations in icy shell thickness and shear modulus caused by that temperature field.

### 3.1.2. Parameters and the Resulting Models

For Europa, we follow *Ojakangas and Stevenson* [1989] and set the obliquity to 1°, the surface albedo to 0.5, and the orbital eccentricity to 0.0094. For Ganymede, we set the obliquity to 0.3°, the surface albedo to 0.43, and the eccentricity to 0.0013. For the basal heat flux, a wide range of values have been used in different studies [see, e.g., *Ojakangas and Stevenson*, 1989; *O'Brien et al.*, 2002; *Nimmo et al.*, 2007]. We choose values that lead to significant lateral variations in the temperature field and shell thickness structure while making sure the mean shell thickness is not large. For Ganymede, the tidal dissipation is relatively weak due to a small orbital eccentricity (0.0013) and a large semimajor axis, and its effects on the spatial pattern of the temperature field can be easily overwhelmed by a large basal heat flux. So to maximize the lateral variability from the tidal dissipation, we prefer to use small basal heating values. However, if we choose a basal heat flux for Ganymede that is too small (e.g., 0.5 mW/m$^2$), we obtain an icy shell that is more than 300 km thick, which would presumably trigger convection in the ice [*Barr and Showman*, 2009]. To avoid convection and to obtain an upper bound estimate for the effects of lateral variability, we use 1 mW/m$^2$ for the basal heat flux and increase the tidal dissipation rate by a factor of 25. By doing so, we have a Ganymede test structure where the lateral variations in the icy shell are significantly amplified and the mean shell thickness (108 km) is reasonably small.

Lateral variations in ice thickness are determined by assuming that the ocean-ice interface occurs along the 250°K isotherm. We show the shell thickness in Figure 1a, and we refer to this model as "GA." The only 3-D variations in model GA are in its icy shell thickness. Although a temperature-dependent shear modulus profile can also be derived based on the same conduction model, we do not include it in model GA. Instead, we will discuss the shear modulus models later in this section.

For Europa, the tidal dissipation rate is relatively large (because of Europa's large 0.0094 eccentricity), so a larger basal heat flux (4.0 mW/m$^2$) is chosen. The shell thickness is shown in Figure 1b. We refer to this 3-D thickness model as "EA." It has a mean thickness of 19.6 km.

As shown in Figure 1, at low and middle latitudes the lateral variability in each satellite's shell thickness is dominated by the tidal dissipation pattern. The tidal dissipation rate is proportional to the square of the tidal strain rate. Since the tidal strain rate is a linear combination of the (2, 0) and (2, 2) harmonics, the nonspherical


©2014. American Geophysical Union. All Rights Reserved.

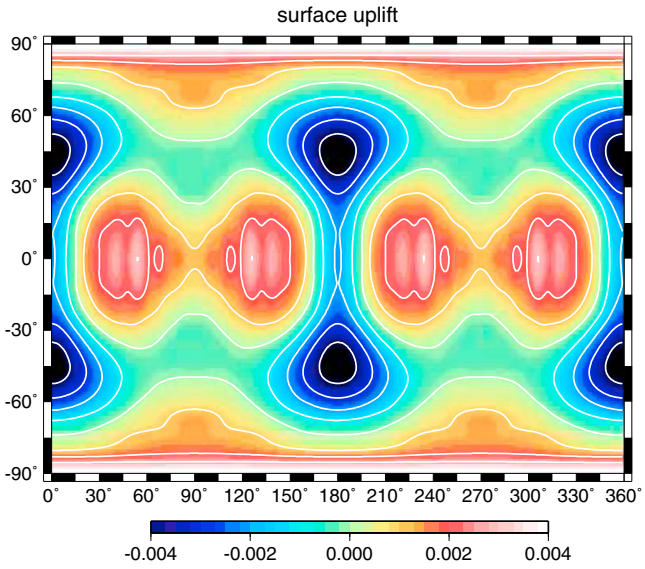


**Figure 2.** The surface uplift of Ganymede in response to a (2, 0) tidal potential. Shown are the difference between the results using model GA (a model of nonuniform ice thickness) and the results using a spherically symmetric model with icy shell thickness equal to the mean for model GA (108 km). The uplift has been normalized by the amplitude of the (2, 0) tidal potential (see text).

components of the shell thickness profile mainly contain terms at (2, 0), (2, 2), (4, 2), and (4, 4). In a small region near the poles, the ice thickness increases with latitude. This polar thickness variability is determined by the surface temperature pattern and is small compared to the lateral variability induced by tidal dissipation. Results of the tidal response for models GA and EA will be discussed in section 4.1.

Using the temperature field derived from the conduction models, we also build temperature-dependent shear modulus profiles for the icy shells of each moon. We assume a linear relation between temperature and shear modulus [*Gammon et al.*, 1983; *Gagnon et al.*, 1988, 1990], given by

$$\mu = 34.1 + 0.07 \times (273 - T), \qquad (2)$$

where $T$ is the temperature in Kelvin and $\mu$ is the shear modulus in kilobar. Applying equation (2) to the temperature field determined by the conduction model, we build shear modulus profiles for Ganymede and Europa. To investigate the effects of the laterally varying shear modulus alone, we assume constant shell thicknesses of 141 km for Ganymede and 27 km for Europa, with each value corresponding to the maximum shell thickness in models GA and EA, respectively. We refer to the resulting models as "GB" for Ganymede and "EB" for Europa, both with a laterally varying shear modulus but constant shell thickness. The results from model GB and EB are presented in section 4.2.1.

### 3.2. Degree-1 Variability in the Shear Modulus of Europa's Outer Shell

The surface of Europa features a hemispherical dichotomy, where the bright leading side contains relatively pure ice, while the reddish trailing side is mixed with ice and hydrated materials. The non-ice material in Europa's outer shell could have been emplaced from the subsurface ocean and/or created by exogenous radiation processing [see, e.g., *Carlson et al.*, 2009]. In the case of exogenic sources, impact gardening and micrometeoric deposition occur mainly on the leading hemisphere [*Zahnle et al.*, 1998, 2003] and the thermal plasma from Io deposits material mostly on the trailing hemisphere [*Alvarellos et al.*, 2008; *Zahnle et al.*, 2008]. A recent spectroscopic study of Europa's surface composition suggests that $MgSO_4$ is present on Europa's trailing side but is absent from its leading side [*Brown and Hand*, 2013].

A hemispherical difference in composition would presumably cause lateral variations in the elastic properties of the icy shell. To investigate whether information about this lateral variability could be gained through tidal measurements and whether the presence of this variability could complicate attempts to learn about the icy shell thickness using tidal observables, we construct a 3-D model where a degree-1 perturbation is added to the shear modulus of Europa's icy shell. To maximize the possible effects of the lateral variability, we assume that the perturbation is present throughout the entire depth of the shell. For simplicity, we assume that the other parameters, including the density, the first Lame parameter ($\lambda$), and the shell thickness, are spherically symmetric.

The degree-1 structure can be written as

$$\mathrm{d}\mu/\mu = -\delta \sin\theta \sin\varphi, \qquad (3)$$

where $\mu$ is the shear modulus in the icy shell, $\delta$ is a positive constant that quantifies the amplitude of the perturbation, and $\theta$ and $\varphi$ are the colatitude and longitude ($\varphi = 0$ is the sub-Jovian meridian). Equation (3)


©2014. American Geophysical Union. All Rights Reserved.

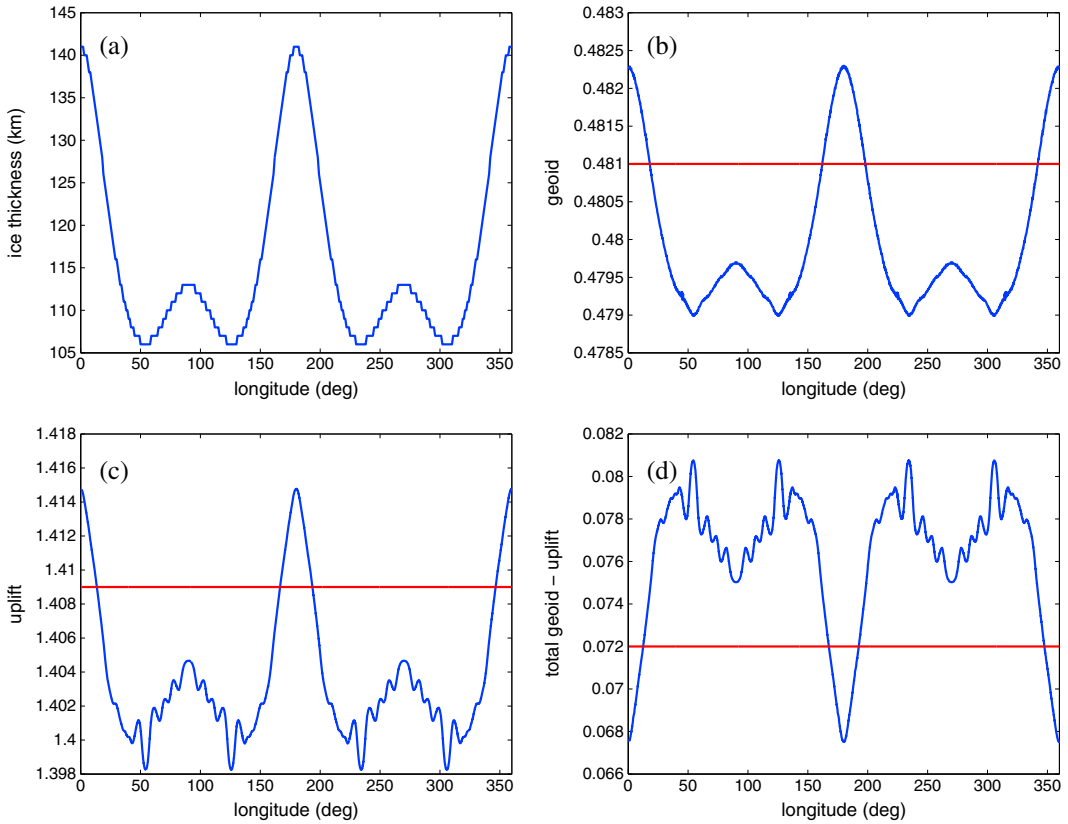


**Figure 3.** The (a) ice thickness, (b) geoid, (c) surface uplift, and (d) difference between total geoid and uplift, for Ganymede model GA (a model of nonuniform ice thickness). Results are from (2, 0) tidal forcing and are plotted along Ganymede's equator. The normalization is described in the text. The horizontal lines in Figures 3b–3d denote the spherically symmetric results.

represents a (1, 1) variation in $\mu$, where the trailing hemisphere has a larger $\mu$ than the leading hemisphere. In this study, we build degree-1 shear modulus profiles using $\delta = 0.5\%$, 1%, 2%, and 4%, and we refer to all these models as "EC." The minimum value of $\delta$ (0.5%) is chosen so that our numerical method is still able to resolve the differences caused by the small variation in shear modulus. In fact, if the hemispherical difference in composition is mainly caused by exogenic processes, the low bombardment rate [*Carlson et al*., 2009], coupled with the fact that adding $MgSO_4$ to the ice is not likely to dramatically change the shell's rheological properties [*Brown and Hand*, 2013], means that even a value as small as $\delta = 0.5\%$ might be an overestimate of the lateral variability in the shear modulus. As we will demonstrate below, results corresponding to smaller and probably more realistic values of $\delta$ can be obtained by linearly scaling the results from model "EC." Details regarding this are discussed in section 4.2.2. For a maximum value, we choose $\delta = 4\%$ mainly to verify the linear relation between the (1, 1) perturbation and the degree-3 tidal solutions (see section 4.2.2).

### 3.3. Grounded Ice on Ganymede

Suppose the liquid ocean on Europa or Ganymede is nonglobal in extent, so that the icy outer shell is grounded in places and floating in others. What impact would that have on the tidal response? To address that question, we take Ganymede as an example. We continue to assume that the rocky mantle is a spherical shell, with its surface at a depth of 2638–1913 = 725 km (see Table 1) beneath Ganymede's outer surface. As a result, a location where the outer shell is grounded means that the ice there extends down all the way to that depth. We offer no physical justification for such a model. Our intent is only to determine whether a partially grounded shell could be detected in tidal observations and how it might complicate attempts to determine the thickness of the floating shell.

We test two hypothetical icy shell structures with grounded ice. For the first model, referred to as GC1, we assume that the icy shell is grounded at longitudes between 0° and 30°. For the second model, referred to as


©2014. American Geophysical Union. All Rights Reserved.

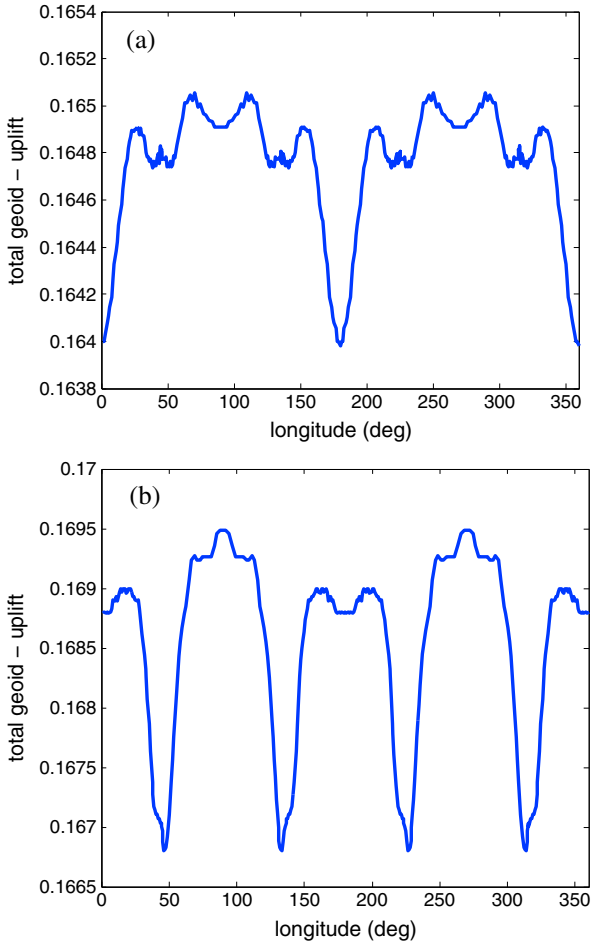


**Figure 4.** The difference between the total geoid and the uplift along the equator, of (a) Ganymede using model GB and (b) Europa using model EB. Both models assume 3-D variations in the icy shell's shear modulus, caused by conduction in the shell. Results are for (2, 0) tidal forcing. The normalization is described in the text.

GC2, the icy shell is grounded at longitudes between 0° and 60°. For both models the thickness of the floating shell is kept uniform (108 km). This grounded ice geometry has been chosen to be symmetric about the equator. This makes the tidal results relatively simple and instructive, and we suspect the general conclusions we infer from the results would be applicable for other geometries as well. Those results are discussed in section 4.3.

## 4. Results

In this section, geoid and uplift results for 3-D models are presented in the spatial domain in Figures 2–6, and in terms of spherical harmonic coefficients in Tables 2 and 3. Figure 2 shows uplift results over the entire surface, whereas the other figures (Figures 3–6) show results only along the equator. For all models, we use a forcing tidal potential $V_T(\theta, \phi) = V_T^0 Y_2^0(\theta, \phi)$, where $Y_2^0(\theta, \phi)$ is the (2, 0) spherical harmonic and the amplitude, $V_T^0$, is a constant.

The results in the figures and tables are normalized as follows. First, we note that for a spherically symmetric satellite, the tidal perturbation in the geoid, $N(\theta,\phi)$, and the tidal uplift of the surface, $U(\theta,\phi)$, are given by

$$N(\theta, \phi) = k_2 V_T^0 Y_2^0(\theta, \phi)/g \quad \text{and}$$
$$U(\theta, \phi) = h_2 V_T^0 Y_2^0(\theta, \phi)/g \qquad (4)$$

where $k_2$ and $h_2$ are the degree-2 Love numbers and $g$ is the surface gravitational acceleration. Throughout this section, we use the term "geoid" to refer to the gravitational contributions caused by tidal deformation in the satellite's interior and "total geoid" to refer to the "geoid" plus contributions from the direct tidal potential from Jupiter. The total geoid, for example, would be $N_{\text{tot}}(\theta, \phi) = (1 + k_2)V_T^0 Y_2^0(\theta, \phi)/g$ for a spherical satellite.

Motivated by equation (4), we normalize the 3-D geoid and uplift solutions along the equator (Figures 3–6), by dividing the geoid and uplift at every location by $V_T^0 Y_2^0(\theta, \phi)/g$. The harmonic $Y_2^0(\theta, \phi)$ is independent of longitude, $\phi$, and so is constant along the equator. With this normalization, the results for $N(\theta,\phi)$ and $U(\theta,\phi)$ for a spherical model would equal $k_2$ and $h_2$, respectively, at all $(\theta,\phi)$. For a 3-D model, the normalized results can thus be compared directly with numerical values of $k_2$ and $h_2$ (0.48 and 1.41 for Ganymede and 0.24 and 1.10 for Europa, using the spherical symmetric models described in Table 1), to gain a sense of the relative importance of 3-D effects.

For Figure 2, which shows the uplift over the entire surface, dividing by $Y_2^0(\theta, \phi)$ would cause problems because $Y_2^0$ vanishes at certain latitudes. Instead, for Figure 2 we divide the uplift by $V_T^0/g$. We also subtract the dominant $h_2 Y_2^0(\theta, \phi)$ term to obtain Figure 2, so that the 3-D effects can be seen more clearly.

For the harmonic coefficients shown in Tables 2 and 3, we divide each coefficient by $V_T^0/g$: i.e., the amplitude of the $Y_2^0(\theta, \phi)$ coefficient of the tidal potential (divided by $g$). The spherical harmonic functions are normalized as described in *Zhong et al.* [2008]. For a spherically symmetric model, the (2, 0) components


©2014. American Geophysical Union. All Rights Reserved.

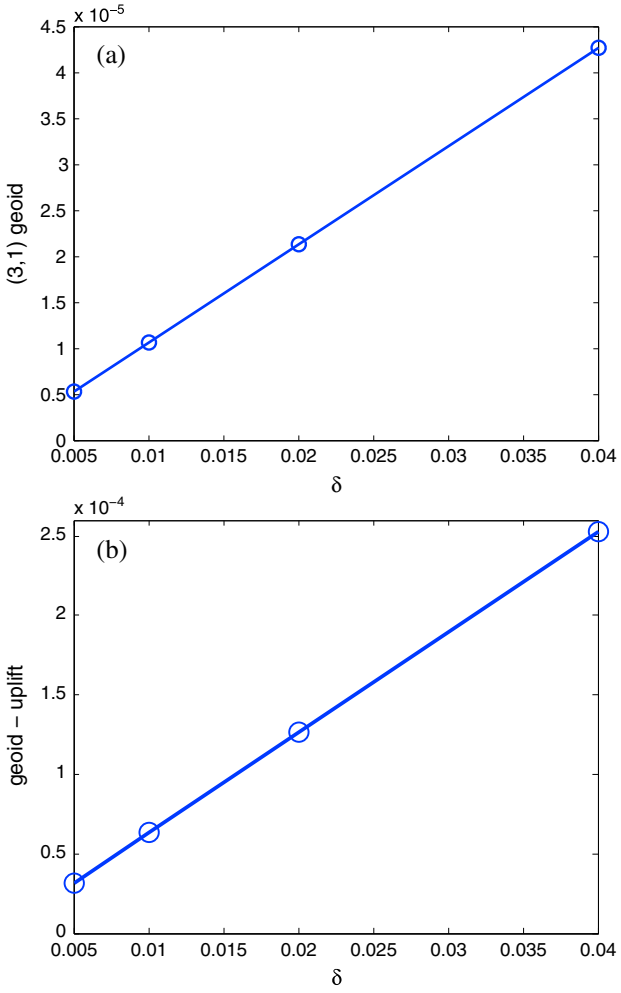


**Figure 5.** The magnitude of the (3, 1) harmonic coefficient of (a) the geoid and (b) the difference between geoid and uplift versus the magnitude of the degree-1 perturbation ($\delta$) in shear modulus, for model EC (hemispherical differences in the icy shell's shear modulus, caused by variations in composition). Results are for (2, 0) tidal forcing. The circles correspond to the results for $\delta = 0.5\%$, 1%, 2%, and 4%. The best fitting line (also included in the figure) passes through the circles, indicating that there is a near-linear dependence of the (3, 1) tidal response on the magnitude of the perturbation. The normalization is described in the text.

of $N$ and $U$ would thus equal the Love numbers $k_2$ and $h_2$, respectively, while the other ($l$, $m$) coefficients would vanish, in principle, although, in practice, numerical noise tends to cause small but nonzero leakage into other harmonics. To construct Tables 2 and 3, we subtract the coefficient values obtained for the spherical models described in Table 1. This not only removes the spherical Love numbers, $k_2$ and $h_2$, from the (2, 0) coefficients but also removes the effects of numerical leakage into the other coefficients. The coefficients shown in the Tables thus represent the effects of 3-D structure. In those tables, we do not include the (2, 0) coefficients (after removing the 1-D results); we will discuss them below in the context of $\Delta_2$.

### 4.1. Results for Laterally Varying Icy Shell Thickness

Using the laterally varying shell thickness model GA and keeping the other satellite properties equal to the spherically symmetric values shown in Table 1, we force the satellite with a (2, 0) tidal potential and compute the tidal response. To offset numerical errors related to leakage from the large (2, 0) response into other harmonics and to highlight the effects of laterally varying shell thickness, we also compute the tidal response using the fully spherical Ganymede model with a shell thickness of 108 km (the mean shell thicknesses of model GA) and subtract the results for that spherical model from the GA results. The geoid and uplift results in the spherical harmonic domain are shown in Table 2 for Ganymede. Before subtracting the spherical model result, the dominant response is at (2, 0) and is about 3 orders of magnitude (or more) larger than the response at the other degrees. After removing the spherical model result, the largest coefficients occur at even-numbered degrees and orders. These results are due to first-order, spherical harmonic coupling between the satellite structure and the (2, 0) tidal potential. As mentioned in section 3.1, the nonspherical components of the icy shell thickness are largely determined by the tidal dissipation rate, which mainly contains terms at (2, 0), (2, 2), (4, 2), and (4, 4). So when this structure is coupled with a (2, 0) tidal potential, the selection rules for products of spherical harmonics [*Edmonds*, 1957] require that the first-order response can occur only at even-numbered degrees and orders.

In reality, the exact tidal potential from Jupiter also contains a large (2, 2) term, in addition to the (2, 0) forcing considered here (see equation (1)). If we were to couple (2, 2) forcing with the nonspherical components of the shell thickness profile, we would expect to obtain a tidal response at even-numbered degrees and orders in that case, too.


©2014. American Geophysical Union. All Rights Reserved.

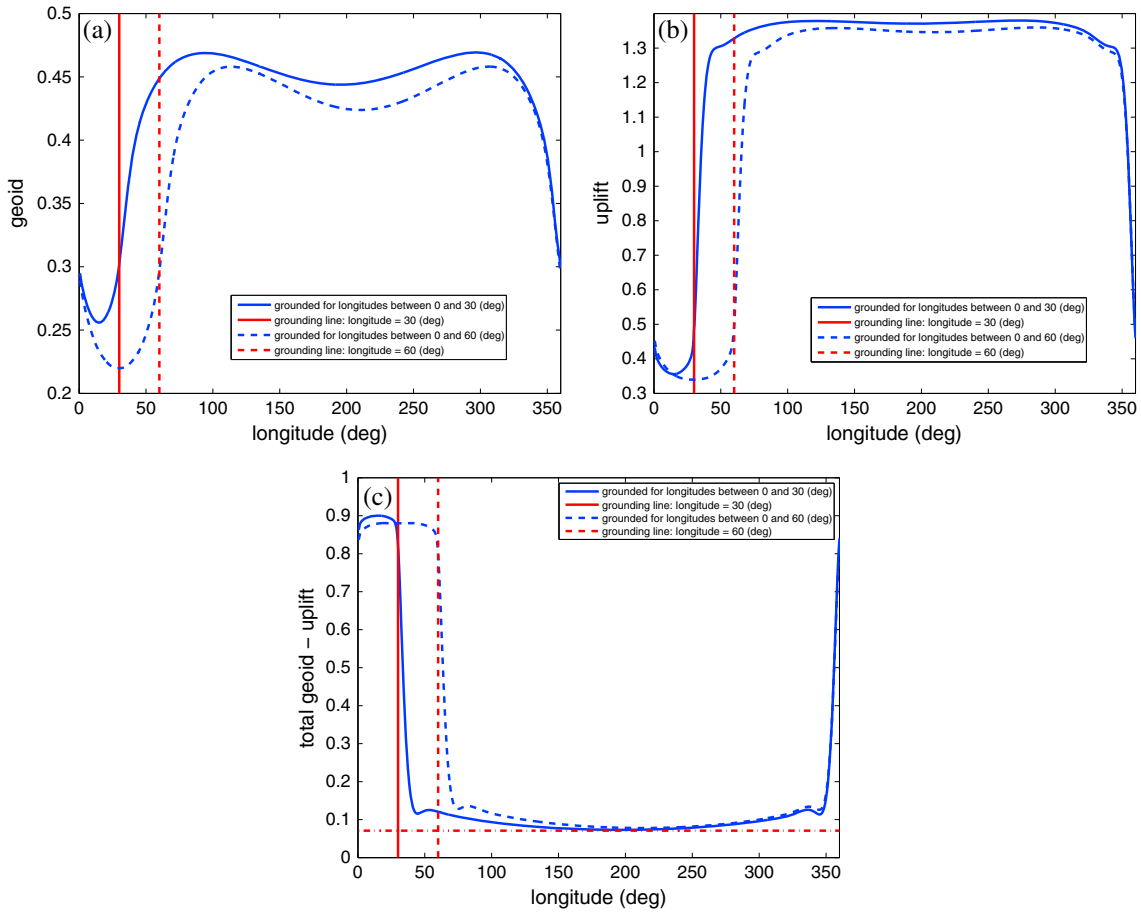


**Figure 6.** (a) Geoid, (b) surface uplift, and (c) difference between the total geoid and uplift, for Ganymede models with a nonglobal liquid ocean. The results are shown as solid and dashed curves for models GC1 (the icy shell is grounded for longitudes between 0° and 30°) and GC2 (the icy shell is grounded for longitudes between 0° and 60°), respectively. The vertical lines show the grounding line positions. In Figure 6c, the dash-dotted line shows the results using a spherically symmetric model with icy shell thickness equal to the mean for model GA (108 km). The results are for (2, 0) tidal forcing and are plotted along Ganymede's equator. The normalization is described in the text.

**Table 2.** The Largest Spherical Harmonic Coefficients of the Geoid and Surface Uplift for Ganymede (Forced by a (2, 0) Tidal Potential)[a]

| Geoid | | | Uplift | | |
|---|---|---|---|---|---|
| (*l*, *m*) | cos | sin | (*l*, *m*) | cos | sin |
| (4, 0) | 7.36E−04 | 0.00E+00 | (4, 0) | 3.32E−03 | 0.00E+00 |
| (2, 2) | −6.23E−04 | −6.27E−09 | (4, 4) | −1.96E−03 | 3.91E−09 |
| (4, 4) | −3.58E−04 | 1.28E−09 | (2, 2) | −1.87E−03 | −3.91E−09 |
| (4, 2) | −2.95E−04 | −1.16E−09 | (4, 2) | −1.32E−03 | −2.00E−09 |
| (6, 0) | 7.68E−05 | 0.00E+00 | (6, 0) | 5.61E−04 | 0.00E+00 |
| (6, 2) | −7.52E−05 | −1.37E−10 | (6, 2) | −5.25E−04 | −2.27E−09 |
| (6, 4) | −6.70E−05 | 6.23E−10 | (6, 6) | −4.95E−04 | 1.23E−09 |
| (6, 6) | −6.04E−05 | −2.85E−10 | (6, 4) | −4.30E−04 | 3.40E−09 |
| (8, 8) | −2.70E−05 | 1.85E−10 | (8, 8) | −2.90E−04 | 6.70E−10 |

[a]The spherical harmonic functions are defined as in *Zhong et al.* [2008]. The coefficients are the differences between the results of model GA (a model of nonuniform ice thickness) and the results from a spherical model with an icy shell thickness equal to the mean thickness of model GA (108 km). The (2, 0) components are not included. The normalization is discussed in the main text. Before removing the spherical model result, the (2, 0) components are 0.48 and 1.41 for the geoid and uplift, respectively.


©2014. American Geophysical Union. All Rights Reserved.

**Table 3.** The Largest Spherical Harmonic Coefficients of the Geoid and Uplift for Europa (Forced by a (2, 0) Tidal Potential)[a]

| Geoid | | | Uplift | | |
|---|---|---|---|---|---|
| (*l*, *m*) | cos | sin | (*l*, *m*) | cos | sin |
| (3, 1) | −8.54E−10 | −4.31E−05 | (3, 1) | −8.94E−09 | −2.99E−04 |
| (2, 2) | −1.64E−06 | 4.63E−10 | (1, 1) | 5.09E−09 | −1.29E−04 |
| (5, 5) | 6.66E−11 | −2.94E−07 | (2, 2) | −8.11E−06 | 4.78E−09 |
| (5, 3) | 4.85E−11 | 2.58E−07 | (5, 5) | 2.89E−09 | −3.47E−06 |
| (3, 3) | 3.12E−10 | 1.63E−07 | (5, 3) | 2.11E−10 | 2.95E−06 |
| (7, 3) | −7.20E−11 | −1.42E−07 | (7, 3) | 2.40E−09 | −2.35E−06 |
| (7, 5) | −6.58E−11 | 1.14E−07 | (7, 5) | −1.17E−09 | 1.81E−06 |
| (9, 1) | −1.38E−10 | 6.15E−08 | (13, 3) | −9.80E−09 | −1.31E−06 |
| (5, 1) | −3.68E−10 | 5.70E−08 | (9, 1) | −4.13E−09 | 1.31E−06 |

[a]The coefficients are the differences between the results for one of the EC models, where compositionally driven (1, 1) structure of amplitude $\delta = 4\%$ is included in the shear modulus of the icy shell and the results for a uniform icy shell. The (2, 0) components are not included. Before removing the spherical background, the (2, 0) components are 0.24 and 1.1 for the geoid and uplift, respectively.

Using the degree-2 tidal solutions, we investigate whether the mean shell thickness could be accurately estimated using observations of degree-2 Love numbers, in the presence of lateral variations in shell thickness. As described in *Wahr et al.* [2006], for a spherically symmetric satellite, the combination of Love numbers,

$$\Delta_2 = 1 + k_2 - h_2, \tag{5}$$

is proportional to the shell thickness (in the case of a thin shell), where the proportionality constant depends on the density of the ocean and the shear modulus of the ice. If the density and shear modulus are known accurately enough, then an estimate of $\Delta_2$ based on observations of $k_2$ and $h_2$ from radio tracking and altimetric observations, respectively, could be used to determine the shell thickness. When the shell thickness is laterally varying, one question to ask is whether an observational determination of $\Delta_2$ would still provide a good estimate of the mean shell thickness.

To address this question, suppose that the icy shell has laterally varying thickness and that $\Delta_2$ is computed using observations of the (2, 0) spherical harmonic coefficients of the geoid and uplift, just as in the spherical case. For Ganymede (model GA), the value obtained for $\Delta_2^{GA}$ would be 0.073, whereas the value for a spherical satellite with the same mean shell thickness is $\Delta_2^{mean} = 0.072$. The relative difference between these numbers is 1.4%, implying that if the observed $\Delta_2$ was used to determine the shell thickness under the assumption of a spherically symmetric satellite, the inferred thickness would differ from the mean shell thickness by 1.4%. For our Ganymede model, where the mean shell thickness is 108 km, this 1.4% effect translates to an error of 1.5 km in the estimated mean shell thickness.

There have been no published estimates of the level of observational error in $\Delta_2$ that could be achieved with a future Ganymede mission. There is, though, a published error estimate for Europa, based on one specific assumed orbital configuration [see *Wahr et al.*, 2006]. In that case, the expected observational error in $\Delta_2$ would be roughly 1%. Although the actual observational error would be mission (and satellite) specific, the suggestion from these numbers is that the error caused by the presence of 3-D shell thickness variations is likely to be of the same order or smaller (we have chosen parameter values in our conduction model that maximize the lateral thickness variations) than the observational error, so we suspect that the presence of conduction driven 3-D variability in shell thickness is not likely to limit attempts to use $\Delta_2$ to constrain the mean icy shell thickness in a significant way.

In Figure 2, we plot the surface uplift of Ganymede in the spatial domain, after removing the spherical model results. The uplift is normalized by the amplitude of the (2, 0) tidal potential but not by its $(\theta, \varphi)$ dependence. Figure 2 thus shows the pattern of the nonspherical response that could be observed by an altimeter. If we choose any fixed longitude and note how the uplift and ice thickness (from Figure 1a) vary in the north-south direction at that longitude, we see that thinner ice tends to experience larger uplifts than the thicker ice. For instance, the icy shell thickness is smaller than average near the poles. The


©2014. American Geophysical Union. All Rights Reserved.

uplift results from the 1-D model are positive near the poles ($Y_{20}$ is positive there), and the differences between the 3-D and 1-D results shown in Figure 2 are positive there, implying that the 3-D uplift of the relatively thin near-polar ice is larger than the uplift for the 1-D case. Near the equator, where the icy shell thickness is larger than average, this is reversed. There, the 1-D uplift results are negative ($Y_{20}$ is negative near the equator), and the differences shown in Figure 2 between the 3-D and 1-D results are mostly positive (except for 0 and 180 longitudes), implying a decreased amplitude of the 3-D uplift on the thicker icy shell.

The spatial pattern of the surface uplift is more complicated, though, when looking at the east-west variability at any fixed latitude. To investigate this in detail, we plot the ice thickness, the geoid, the surface uplift, and the difference between the total geoid and the uplift, all along Ganymede's equator, in Figure 3. Figures 3b–3d are normalized as described above in the first paragraphs of section 4. To show the relative amplitude of the spatial variability, we do not remove the results from the spherically symmetric model, and we plot the spherically symmetric results using a horizontal line. Because the spherically symmetric model results consist solely of a (2, 0) component, those results are constant along the equator, and so their contributions are to add a longitude-independent constant to each figure. The geoid and uplift results (Figures 3b and 3c) clearly show the same order-2 and order-4 patterns (i.e., $\cos 2\varphi$ and $\cos 4\varphi$ longitude dependence, respectively) that are present in the ice thickness structure (Figure 3a). But the sign of how the uplift varies along this east-west transect is the opposite of what we might expect: regions of thick ice experience large uplift and regions of thin ice experience small uplift.

The uplift has much larger spatial variability than the geoid. As a result, the difference between the total geoid and the uplift (that difference would be equal to $\Delta_2 = 1 + k_2 - h_2$ for a spherical satellite) mostly reflects the negative of the uplift. We define this difference as $\Delta(\theta, \varphi)$. In contrast to the spherically symmetric case, where $\Delta$ is linearly proportional to the thickness of the icy shell, results from our laterally varying shell thickness model do not show a linear relation between $\Delta(\theta, \varphi)$ and the ice thickness that is valid for every $(\theta, \varphi)$ (compare Figure 3d with 3a).

Summarizing the results for laterally varying shell thickness, results in the spherical harmonic domain show that the nondegree-2 harmonics in the tidal solution are determined by first-order coupling between the tidal potential and lateral variations of the icy shell thickness. Gravity observations of the geoid or altimetric observations of the uplift could be used to detect the presence of 3-D shell structure, if those observations were sufficiently accurate. Inverting for details of that structure, though, would likely be difficult. For example, if laterally varying shell thickness exists, we find that a smaller value of uplift does not necessarily correspond to a locally thicker shell, which would complicate efforts to use detailed altimeter measurements of the spatially dependent uplift to infer the pattern of 3-D icy shell thickness. On a positive note, if radio tracking and altimetric observations could be used to resolve the degree-2 gravity and uplift coefficients, the mean shell thickness could be estimated from $\Delta_2$ using an approach developed for a spherically symmetric interior, even in the presence of variable thickness.

In this section, we do not include results using model EA mainly because we could not achieve the same level of numerical convergence as in the model GA results (see Appendix A for a detailed description of the numerical properties of our finite-element solutions). However, because model EA has a much smaller mean shell thickness than model GA, so that the EA lateral variations in thickness (which have roughly the same amplitude relative to the mean thickness, as the GA lateral variations) are much smaller than those for GA, we suspect that the 3-D effects from model EA are likely to be even smaller than those from model GA.

### 4.2. Results for a Laterally Varying Shear Modulus in the Icy Shell

#### 4.2.1. Temperature-Dependent Shear Modulus Derived From the Conduction Model

We compute the response to a unit amplitude (2, 0) tidal potential using models GB for Ganymede and EB for Europa. Similar to the results from the model (GA) with laterally varying icy shell thickness, only even degrees and orders appear in the solutions, and the (2, 0), (2, 2), (4, 2), and (4, 4) terms dominate. This is not surprising since the laterally varying shear modulus profiles are derived from the same temperature fields used to generate the shell thickness models.

The difference between the total geoid and uplift (equal to $\Delta_2 = 1 + k_2 - h_2$ for a spherically symmetric satellite) along the equator is plotted in Figures 4a and 4b for models GB and EB, respectively. Similar to


©2014. American Geophysical Union. All Rights Reserved.

the 3-D shell thickness results, order-2 and order-4 patterns are evident, but their amplitudes are much smaller than those for model GA (compare with Figures 3d). This suggests that a laterally varying shear modulus is likely to have a smaller impact on the tidal response than laterally varying icy shell thickness. We suspect that this general conclusion is true if the shear modulus profile and the shell thickness structure are determined using any conduction model. However, caution needs to be exercised if there is viscous flow in the icy shell, since that tends to reduce the lateral variability in shell thickness, which would cause the effects of a laterally varying shear modulus to become relatively more important.

#### 4.2.2. Compositional-Dependent Degree-1 Variability in the Shear Modulus of Europa's Icy Shell

Using the degree-1 shear modulus structure from model EC, we compute Europa's response to (2, 0) tidal forcing for different 3-D amplitudes: i.e., for $\delta = 0.5\%$, 1%, 2%, and 4%. Again, we remove the spherically symmetric solution from the results. Table 3 shows the largest spherical harmonic coefficients when $\delta = 4\%$, for both the geoid and the uplift. The largest nondegree-2 response is at (3, 1). This can be understood in terms of first-order coupling between the (2, 0) forcing and (1, 1) structure. To first order, the response is at (3, 1) and (1, 1), and their magnitudes should be proportional to the amplitude of the (1, 1) perturbation in the shear modulus (i.e., to $\delta$). Since our geoid results are computed in the center of mass frame, the degree-1 potential vanishes. For the uplift, both the (1, 1) and (3, 1) terms are among the largest, with the (1, 1) component being about 4 times smaller than the (3, 1) component. In Figure 5a, the magnitude of the (3, 1) term in the geoid is plotted versus the amplitude of the perturbation. A linear relation is evident, which is additional evidence that the 3-D compositional effects are first order, at least for this range of 3-D amplitudes. There is a similar linear dependence for the uplift (not shown here).

We compute $\Delta_2 = 1 + k_2 - h_2$ for model EC with $\delta = 4\%$, and we find that the difference in $\Delta_2$ between the model EC result and the spherical symmetric result is less than $10^{-5}$, which is considerably smaller than the corresponding result computed for the laterally varying shell thickness model (see section 4.1). This means that the effects of compositionally driven shear modulus variability on measurements of $\Delta_2$ would be smaller than those described for the 3-D shell thickness model. And as argued above, even the effects of 3-D shell thickness are too small to have a significant impact on estimates of mean shell thickness obtained from observations of $\Delta_2$.

Using these results, we investigate whether (1, 1) structure in the shear modulus could be detected using observations of the degree-3 tidal response. One complication is that the exact (3, 1) tidal response should contain two components: (a) the (3, 1) response caused by first-order coupling between the (2, 0) tidal potential and the (1, 1) perturbation in the shear modulus (i.e., the (3, 1) response computed in this section) and (b) the direct response to the (3, 1) tidal potential. To expand on (b), the exact tidal potential from Jupiter includes spherical harmonics of all degrees, including a (3, 1) term. To lowest order, Europa's response to this or any other tidal forcing term (including the (2, 0) term considered in this paper) can be estimated by assuming Europa is spherically symmetric.

For (a), the (3, 1) term in the geoid, shown in Figure 5a, has a magnitude of $\sim 4.3 \times 10^{-5}$ when $\delta = 4\%$ and of $5.3 \times 10^{-6}$ if $\delta = 0.5\%$. For the contribution from (b), the amplitude of a degree-$l$ component of the tidal potential is smaller than the degree-2 amplitude by a factor of [Europa's radius/Europa-Jupiter distance]$^{l-2}$ [e.g., *Agnew*, 2008] (equation (4)), implying that the degree-3 forcing terms are smaller than the degree-2 terms by a factor of $\sim 430$. Using our spherically symmetric model, we find that the degree-3 potential Love number for Europa is 0.17. This suggests that the contribution from (b) is $\sim 3.8 \times 10^{-4}$. So even if the degree-1 perturbation in the shear modulus is as large as 4%, the effect of this lateral variability on the geoid would be nearly 1 order of magnitude smaller than the spherical response to the degree-3 tidal forcing. The conclusions are similar for the (3, 1) term in the uplift, implying that it might be challenging to use the (3, 1) geoid or uplift alone to detect a (1, 1) structural term in the shear modulus. However, if we choose the difference between the (3, 1) geoid and the (3, 1) uplift as our observable, we find that for (a), the difference between the geoid and uplift, shown in Figure 5b, is $\sim 2.5 \times 10^{-4}$ if $\delta = 4\%$ and is about $3.2 \times 10^{-5}$ if $\delta = 0.5\%$. For (b), we find that the difference between the degree-3 potential Love number and the uplift Love number (i.e., the difference between the geoid and the uplift) to be ~0.025, implying that the contribution from (b) is $\sim 5.8 \times 10^{-5}$. This value is larger than the contribution from (a) by a factor of ~1.8 if $\delta = 0.5\%$ and is $\sim 23\%$ of the contribution from (a) if $\delta = 4\%$. So when we choose the difference between the (3, 1) geoid and the (3, 1) uplift as our observable, the relative effect of the lateral variability


©2014. American Geophysical Union. All Rights Reserved.

is amplified and is comparable to the spherical response to the degree-3 tidal forcing, for the range of 3-D amplitudes we have investigated.

For a future Europa mission, if an estimate of the mean shell thickness, e.g., through a determination of $\Delta_2$, is available, the response to the degree-3 tidal forcing could be computed using a spherically symmetric Europa model using that estimated mean shell thickness value. By removing this contribution from the total degree-3 geoid and uplift measurements and by estimating the difference between the degree-3 geoid and uplift, the effect of the degree-1 perturbation in the icy shell structure could then conceivably be extracted, leading to an observational constraint on that structure. As argued in section 3.2, the amplitude of the degree-1 structure in the shear modulus is probably small, and even $\delta = 0.5\%$ might be an overestimate of the amplitude of the lateral variability. This implies that the detection of the corresponding 3-D effects would likely be challenging. Its success would require accurate modeling of the direct response to degree-3 tidal forcing and a precise measurement of the degree-3 tidal terms.

### 4.3. Results Using Grounded Icy Shell Models

Using the grounded icy shell models GC1 and GC2, we compute Ganymede's response to (2, 0) tidal forcing. Equatorial values of the geoid, uplift, and difference between the total geoid and uplift are shown in Figure 6 for both models. Where the shell is grounded the geoid and uplift are consistently smaller than where it is floating. For the uplift there is a sharp delineation between grounded and floating regions, with floating values being more than 3 times larger than grounded values. The geoid shows more large scale variability: there is no sharp delineation between grounded and floating regions, and the relative variation is smaller (less than a factor of 2). This is because surface gravity is determined by the deformation of the entire satellite. The mass related to the large uplift in the floating region, for instance, can have an impact on the gravity signal above the grounded ice.

The large-scale geoid variability also shows up to some extent in the uplift, because of the tendency of the liquid ocean to lie along a surface of constant potential (the geoid). So when the uplift is removed from the total geoid to obtain $\Delta(\theta, \varphi)$, the results (Figure 6c) show an even more pronounced floating/grounded difference than the uplift.

The spatial variability obtained here for models GC1 and GC2 is significantly larger than that for the other 3-D models, in which the subsurface ocean is global. The variability is dramatic enough to suggest that observations of spatial variations in the tidal observables, especially in the surface uplift and in the difference between the total geoid and uplift, could be used to identify regions where the icy shell is grounded.

Suppose that the icy shell is, indeed, partially grounded, and altimeter tidal observations were able to roughly outline the floating region. Could combined altimeter/radio tracking observations of $\Delta(\theta, \varphi)$ over just the floating region be able to determine the floating shell's thickness, as has been proposed for a spherical satellite (see section 4.1)? In Figure 6c, we show $\Delta(\theta, \varphi)$ along the equator for models GC1 and GC2. As a comparison, we also calculate $\Delta(\theta, \varphi)$ of a fully spherical satellite model with a shell thickness of 108 km (which equals the floating shell's thickness), shown as a horizontal line in Figure 6c. Comparing the 3-D and 1-D results, we find that the existence of grounded ice tends to increase the difference between the total geoid and uplift over the floating region. If we use this difference to estimate the thickness of the floating icy shell, we are likely to obtain an estimate that is somewhat too large. An estimate that is closer to the true value may be obtained by restricting the observations to regions farther away from the grounded ice. But even then, the inferred ice thickness would probably be somewhat overestimated.

## 5. Conclusions and Discussion

In this study, we use a finite-element model to solve for the tidal response of Ganymede and Europa using various icy shell models with laterally variable structures. In all cases, the shell is assumed to lie above a liquid-water ocean. Icy shell structures with significant laterally varying shell thickness are derived from a thermal conduction model. Three-dimensional structures of the shear modulus within the shell are built either from a conduction model or, for Europa, by postulating a hemispherical difference in composition. For each model, we choose amplitudes of the lateral variability that are plausible, but large. We also build icy shell structures for Ganymede where we assume a nonglobal ocean, so that the shell is partially grounded in places and floating in others. Results based on these test models provide upper bound estimates for the effects of 3-D


©2014. American Geophysical Union. All Rights Reserved.

shell structure on the tidal response and help to determine the likely limitations of future efforts to infer shell structures from tidal measurements.

Relevant to those measurements, the most pertinent general questions are as follows: (1) would the presence of any of these structures complicate efforts to determine the existence or absence of an underlying liquid ocean? (2) Would the effects of those structures on the degree-2 Love numbers ($k_2$ and $h_2$) be small enough that the mean shell thickness could still be accurately estimated from measurements of $\Delta_2(= 1+ k_2 - h_2)$, as has been argued in the past for a spherically symmetric icy satellite? (3) Could tidal measurements be used to learn anything about those structures? Here we summarize the answers to those questions for each type of 3-D structure considered in this paper.

Results from model GA show that the nondegree-2 harmonics in the geoid are determined by first-order coupling between the tidal potential and lateral variations in the thickness. The effects of variable thickness on the degree-2 Love numbers are considerably smaller than the effects of a liquid ocean. For example, we find that for Ganymede, $k_2$ and $h_2$ would equal ~0.48 and ~1.41 if there is a liquid ocean and ~0.11 and ~0.23 if there is not. Those differences are far larger than the effects of lateral thickness variations on the (2, 0) geoid and uplift components. Because the parameter values used to construct model GA were chosen to maximize those thickness variations, we conclude that the presence of lateral variability in thickness would not obscure the effects of a liquid ocean in radio tracking observations of tidal gravity perturbations or in altimeter observations of tidal uplift. In fact, the 3-D perturbations on the (2, 0) components for model GA are small enough that the mean shell thickness could be meaningfully estimated from observations of $\Delta_2 = 1 + k_2 - h_2$ using methods derived for a spherically symmetric satellite, as described above. Since the 3-D lateral variability in model EA is smaller than that in model GA, we suspect that these conclusions are the same for Europa.

It is possible that given sufficient measurement accuracy, radio tracking observations of nondegree-2 tidal harmonics or altimeter observations of nondegree-2 tidal surface displacements could be used to infer that lateral variability in shell thickness does exist. Using those observations to place constraints on that variability, though, would probably be difficult, because the spatial pattern of the tidal deformation includes features that do not necessarily mirror the thickness variability. For example, locations that exhibit a smaller value of uplift than average do not necessarily correspond to locations with a thicker-than-average shell (see Figure 2).

Using shear modulus profiles for the icy shell derived from the same conduction models used to estimate the lateral thickness variations, we find similar first-order harmonic coupling effects as for the models with 3-D shell thickness. We also find that unless there are additional mechanisms (such as viscous flow in the icy shell) that act to reduce the lateral variations in thickness, the effects of a laterally varying shear modulus on the tidal response are likely to be smaller than those of a laterally varying shell thickness. We conclude that as for the case of laterally varying thickness, the presence of a conductive-driven 3-D variations in shear modulus would not degrade attempts to deduce the existence or absence of a liquid ocean using tidal observations, would not significantly impact attempts to infer mean shell thickness from observations of $\Delta_2$, and could probably not be mapped out with confidence using nondegree-2 gravity or altimeter observations.

To represent possible hemispherical differences in the composition of Europa's icy shell, we include (1, 1) structure in the shear modulus of the ice. Forcing this 3-D structure with a (2, 0) tidal potential, we find a (3, 1) pattern in the surface response, with an amplitude that is proportional to the amplitude of the (1, 1) perturbation in the shear modulus. In general, the tidal potential of Europa contains large (2, 0) and (2, 2) terms, along with smaller terms at other degrees and orders. If a (1, 1) structure in the shear modulus were to be coupled with the exact diurnal tidal potential, the dominant response caused by that structure would occur at harmonics (3, 1) (for (2, 0) and (2, 2) forcings) and (3, 3) (for (2, 2) forcing). This structure would not impact attempts to infer the existence of a liquid ocean nor would it have a significant effect on mean shell thickness inferred from observations of $\Delta_2$.

The question of whether the degree-3 response caused by any such (1, 1) structure could be extracted from observed degree-3 tidal solutions depends on the magnitude of the structure, the accuracy of the measurements, and whether there are other types of lateral heterogeneities that could introduce a degree-3 tidal response. As described in section 4.2.2, any future interpretation of observed degree-3 tidal terms would require accurate modeling of the satellite's spherically symmetric response to degree-3 tidal forcing. One encouraging conclusion that can be inferred from our results is that conductively driven 3-D structures would


©2014. American Geophysical Union. All Rights Reserved.

induce a significant tidal response only at even degrees and orders, so they would not affect attempts to detect (1, 1) structure through degree-3 tidal measurements. However, if there exist other sources of order-1 lateral variability in Europa's icy shell, probably also caused by compositional heterogeneity (for instance, a high-degree order-1 structure in the shear modulus or a (1, 1) structure in satellite rheological properties other than the shear modulus), they would also induce (3, 1) and (3, 3) responses in the tidal solutions. So for a future Europa mission, the accurate interpretation of the degree-3 tidal measurements requires careful investigation of all possible lateral heterogeneities caused by compositional differences within the icy shell.

The generation of a degree-3 tidal response for a planetary body with degree-1 elastic structure is similar to what *Zhong et al*. [2012] found for a possible degree-1 mantle structure on the Earth's Moon using the same finite-element modeling method as in this study. As in *Zhong et al*. [2012], we find that degree-1 structure also causes changes in the degree-2 tidal response. The linear dependence of the degree-3 tidal response on the amplitude of the perturbed structure (Figure 6) is the result of first-order coupling between the degree-2 tidal force and the assumed degree-1 structure, as predicted by perturbation theory [*Qin et al*., 2013]. However, the mode-coupling rules imply that changes in the degree-2 response cannot possibly be due to first-order coupling [e.g., *Zhong et al*., 2012]. Instead, *Qin et al*. [2013] show that any change in the degree-2 response must be a consequence of second-order coupling. We anticipate that *Qin et al*.'s [2013] perturbation approach could be applied in the future to study problems similar to those explored here.

Using models with a nonglobal ocean, we find that the tidally induced surface uplift is much smaller (more than 3 times smaller for our assumed geometries) in the grounded region than in the floating region. In general, the uplift in floating regions tends to have a slightly smaller amplitude than the uplift of a spherically symmetric satellite with a liquid ocean, and the uplift in grounded regions tends to have a slightly larger amplitude than the uplift of a spherically symmetric satellite without a liquid ocean. Because of this dramatic difference in tidal uplift across the surface, it would presumably be possible to infer the existence of a nonuniform ocean from uplift observations and even to roughly map out its areal extent. The same might be true for tidal gravity observations, though the fact that tidal gravity observations would almost certainly be made in the spherical harmonic domain would make this more challenging. A grounded icy shell tends to increase the difference between total geoid and uplift, even in the floating region, so that an estimate of the mean thickness of the floating icy shell based on this difference (i.e., on $\Delta(\theta, \varphi)$) would likely be too large.

## Appendix A

In Appendix A1, we benchmark the finite-element results where the ocean layer is treated as a low-viscosity region, against semianalytic solutions where the ocean is treated as an inviscid fluid. We discuss in detail how the numerical resolution controls the accuracy of the viscoelastic solution. In our numerical experiment, we find that the finite-element solutions for models with laterally varying shell thickness are susceptible to short-wavelength numerical noise, mainly caused by large lateral viscosity contrasts across different elements in the finite-element grid. In Appendix A2, we discuss the convergence of our 3-D numerical results, and we demonstrate that the short-wavelength numerical noise is reduced by increasing the resolution.

For the case of a laterally variable shear modulus, there is no lateral viscosity contrast, and we have not observed any significant short-wavelength noise. For Appendix A3, we compute the tidal solutions for a (1, 1) shear modulus structure in the ice using two models with different resolutions. We show the agreement between results from those two models.

For the grounded ice cases, we do not observe short-wavelength noise. In Appendix A4, we compute the surface uplift results using model GC1, with two resolution configurations, and show the agreement between those results.

### A1. Benchmark Tests for $h_2$ and $k_2$, by Comparing With Results From the Semianalytic Method

In this section, we compute the body tide Love numbers $h_2$ and $k_2$ using our viscoelastic finite-element model and benchmark the numerical results against semianalytic solutions. The semianalytic solution is based on a standard algorithm that computes the Love numbers for a stratified, compressible, and self-gravitating Earth. This method can include internal, inviscid fluid layers in a rigorous manner and has been used to address the tidal loading problem of Europa in previous studies [see, e.g., *Wahr et al*., 2006, 2009]. For the finite-element model, we assume (as discussed in the main text) that the rocky mantle, liquid ocean, and icy shell are all


©2014. American Geophysical Union. All Rights Reserved.

**Table A1.** Results for the Love Numbers $h_2$ and $k_2$ Obtained Using the Semianalytic and Finite-Element Methods[a]

| | Case ID | Number of Elements in the Horizontal Direction | Number of Elements in the Ocean Layer | Number of Elements in the Ice | Number of Elements in the Rock | $h_2$ | $k_2$ |
|---|---|---|---|---|---|---|---|
| Semianalytical results | | | | | | 1.440 | 0.495 |
| Finite-element results | A1 | 12×48×48 | 18 | 14 | 48 | 1.325 | 0.456 |
| | A2-1D | 12×48×48 | 38 | 10 | 32 | 1.398 | 0.477 |
| | A3-1D | 12×48×48 | 44 | 14 | 22 | 1.399 | 0.478 |
| | A4-1D | 12×80×80 | 44 | 14 | 22 | 1.409 | 0.481 |
| | A2 | 12×48×48 | 26 | 22 | 32 | 1.396 | 0.477 |
| | A3 | 12×48×48 | 26 | 32 | 22 | 1.396 | 0.477 |
| | A4 | 12×80×80 | 26 | 32 | 22 | 1.407 | 0.480 |

[a]For the finite-element results, in cases A1, A2-1D, A3-1D, and A4-1D, we use a uniform icy shell, with thickness equal to 108 km (the mean shell thickness of model GA); in cases A2-A4, we use model GA.

Maxwell viscoelastic solids, and we assign a low viscosity ($10^{11}$ Pa s) to the ocean layer and a high viscosity ($10^{20}$ Pa s) to the ice and rocky mantle. We apply a static (2, 0) tidal forcing to a spherically symmetric Ganymede model with an icy shell thickness of 108 km (the mean thickness of model GA) and compute the tidal Love numbers using four different finite-element grids. We use a static forcing because our goal is to find the elastic body tide Love numbers. The case IDs are referred to as A1, A2-1D, A3-1D, and A4-1D, and the grid setup is described in Table A1. For each of these cases, we use 80 elements in the vertical direction, but we vary how those elements are distributed among the ice, ocean layer, and rocky mantle. In addition, by comparing A3-1D and A4-1D we can also test the effects of different horizontal resolutions.

Before we compare our finite-element results with the semianalytic solution, we test the convergence of the viscous relaxation. The ocean layer's characteristic relaxation time, $\tau_o$, is the ratio of the viscosity to the shear modulus. We use $10^{11}$ Pa s for the viscosity and 2 GPa for the shear modulus (the same shear modulus value as for the ice) in the ocean layer, giving a value of $\tau_o$ equal to 50 s. The relaxation times in the ice and rock are about 8 orders of magnitude larger than $\tau_o$, due to the much larger viscosity we use for those layers ($10^{20}$ Pa s). After we relax the system viscously for hundreds of $\tau_o$, the ocean layer reaches its fluid limit while the other parts of the mantle still behave elastically, and the tidal deformation at the surface converges to a constant value. This convergence is shown in Figure A1, where we plot the time-dependent tidal Love number $h_2$ as a function of the model run time, for cases A1, A3-1D, and A4-1D. The results from case A2-1D are nearly identical to those from case A3-1D and are not shown in the figure. By looking at the slopes of the results near the ends of the run times, we see that the results from case A1 have not quite reached convergence. We suspect the reason is that A1 has low resolution in the ocean layer (there are only 18 elements in the A1 ocean layer; see fourth column of Table A1). After we increase the resolution in the ocean layer, as in cases A3-1D and A4-1D, we obtain good convergence after ~$10^3$ $\tau_o$.

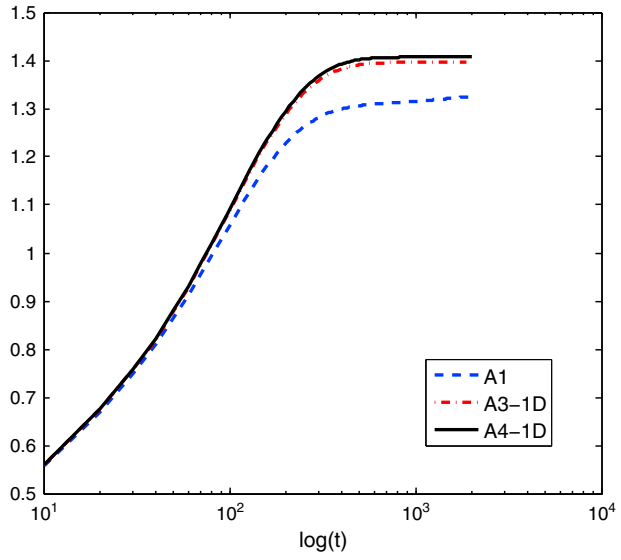


**Figure A1.** The Love number $h_2$ as a function of the logarithm of the model run time for cases A1, A3-1D, and A4-1D. The run time has been normalized by the Maxwell time of the low-viscosity layer (50 s).

Next, we compare our finite-element results with the semianalytic solution and discuss how the resolution controls the accuracy of the numerical results. As shown in Table A1, when we use


©2014. American Geophysical Union. All Rights Reserved.

**Table A2.** Dominant Spherical Harmonic Coefficients of the Surface Uplift[a]

| A2–"A2-1D" | | | A3–"A3-1D" | | | A4–"A4-1D" | | |
|---|---|---|---|---|---|---|---|---|
| (4, 0) | 3.33E−03 | 0.00E+00 | (4, 0) | 3.44E−03 | 0.00E+00 | (4, 0) | 3.32E−03 | 0.00E+00 |
| (4, 4) | −1.99E−03 | −5.96E−10 | (4, 4) | −2.04E−03 | −1.79E−09 | (4, 4) | −1.96E−03 | 3.91E−09 |
| (2, 2) | −1.83E−03 | −2.78E−09 | (2, 2) | −1.85E−03 | 3.64E−09 | (2, 2) | −1.87E−03 | −3.91E−09 |
| (4, 2) | −1.39E−03 | −1.96E−09 | (4, 2) | −1.39E−03 | −2.33E−09 | (4, 2) | −1.32E−03 | −2.00E−09 |
| (6, 0) | 5.57E−04 | 0.00E+00 | (6, 2) | −5.53E−04 | 5.98E−09 | (6, 0) | 5.61E−04 | 0.00E+00 |
| (6, 2) | −5.40E−04 | 1.93E−09 | (6, 6) | −5.15E−04 | −9.97E−10 | (6, 2) | −5.25E−04 | −2.27E−09 |
| (6, 6) | −5.11E−04 | −9.95E−10 | (6, 0) | 4.65E−04 | 0.00E+00 | (6, 6) | −4.95E−04 | 1.23E−09 |
| (6, 4) | −4.41E−04 | 7.60E−10 | (6, 4) | −4.59E−04 | 7.18E−09 | (6, 4) | −4.30E−04 | 3.40E−09 |
| (8, 8) | −2.90E−04 | −1.31E−09 | (8, 8) | −4.14E−04 | −9.35E−09 | (8, 8) | −2.90E−04 | 6.70E−10 |

[a]The (2, 0) coefficients are not included. The coefficients are the difference between the 3-D results using model GA and the 1-D results using a shell thickness equal to the mean thickness of model GA (108 km). We use the same normalization as in Table 2.

$12 \times 48 \times 48$ elements in the horizontal direction and assign only 18 elements in the ocean layer (case A1), we have an error of nearly 8% for the degree-2 Love numbers, as inferred by comparing with the semianalytic solution. If we increase the number of elements in the ocean layer from 18 to 38 (case A2-1D), the error in $h_2$ drops to ~3%, and the error in $k_2$ is now less than 4%. Going from case A2-1D to case A3-1D by increasing the number of elements in the outer icy shell leads to only modest improvements in the solutions. For case A4-1D, we use the same grid setup in the vertical direction as for case A3-1D and increase the horizontal resolution from $12 \times 48 \times 48$ to $12 \times 80 \times 80$. By doing so, the error is reduced to ~2% for $h_2$ and less than 3% for $k_2$. The results of the resolution test indicate that increasing the grid resolution can help improve the accuracy of the numerical results and that the accuracy of the degree-2 tidal solutions is most sensitive to the vertical resolution in the ocean layer. For the 1-D results presented in the main text, we use those from case A4-1D, which is the highest resolution we can currently implement.

### A2. Resolution Test of the Numerical Model for the Case of 3-D Icy Shell Thickness Variations

In this section, we use model GA for 3-D variations in Ganymede's icy shell thickness and compute the tidal response of Ganymede to (2, 0) tidal forcing using three different finite-element grids. The grid setup is shown in Table A1. These 3-D cases are referred to as cases A2, A3, and A4. They have the same horizontal and vertical grid spacings as cases A2-1D, A3-1D, and A4-1D, respectively. The distribution of vertical spacings between nodes is the same for every horizontal location. For a 3-D thickness model, where the ice thickness might be different at one horizontal location than at another, the number of vertical nodes within the ice might be different at different horizontal location. For cases A2-A4, the number of elements in the ice given in the fifth column in Table A1 refers to the number of vertical elements lying within the thickest part of the ice. For case A3, we assign 10 more elements to the ice than in case A2. Those additional elements are concentrated in the lower portion of the icy layer, so that they increase the number of elements at depths lying between the thinnest and thickest parts of the ice. This allows the model to better resolve the 3-D icy shell structure. From case A3 to case A4, we fix the vertical resolution and increase the number of elements in the horizontal direction from $12 \times 48 \times 48$ to $12 \times 80 \times 80$, to investigate the effects of horizontal resolution.

The tidal solutions in the spherical harmonic domain are shown in Table A1 for $h_2$ and $k_2$ and in Table A2 for the dominant spherical harmonic coefficients at other degrees and orders. We find that the 3-D results for $h_2$ and $k_2$ are close to their corresponding 1-D results. The tidal response at other degrees and orders is dominated by long-wavelength terms (degrees 2, 4, 6, and 8), and the difference between the results from cases A2, A3, and A4 are small, implying that the numerical results have converged for the three finite-element grids. In Figure A2, we show the spherical harmonic coefficients of the surface uplift at (2, 2), (4, 0), (4, 2), and (4, 4), as a function of the logarithm of the model run time, for case A4. The results are similar for case A2 and A3, which are not shown here. For each spherical harmonic, the viscoelastic results have converged in the time domain.


©2014. American Geophysical Union. All Rights Reserved.

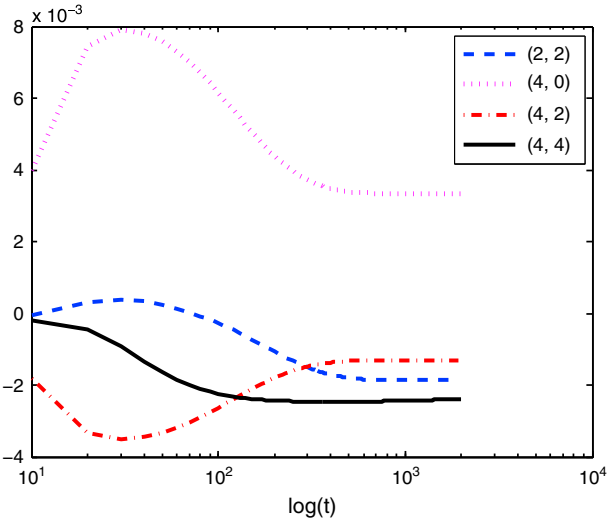


**Figure A2.** The (2, 2), (4, 0), (4, 2), and (4, 4) spherical harmonic coefficients of the surface uplift, as a function of the logarithm of the model run time. The results are for case A4. The run time has been normalized by the Maxwell time for the low-viscosity layer (50 s).

The surface uplift results are plotted along the equator of Ganymede in Figure A3, for cases A2–A4, after subtracting the results from the corresponding spherically symmetric case (A2-1D–A4-1D) to remove the dominant (2,0) component. By comparing the results from cases A2 and A3, we see that by increasing the number of elements that lie between the thinnest and thickest parts of the ice, we have reduced the short-wavelength noise and obtained a smoother solution. By comparing cases A3 and A4, we see that increasing the horizontal resolution has only a modest effect on the short-wavelength features of the solution. The close agreement between the equatorial results shown in Figure A3 is consistent with the good agreement between spherical harmonic results shown in Table A3. For the model GA results presented in the main text, we use those from case A4, which is the highest resolution we can implement.

For model EA of Europa, we could not achieve the same level of convergence in the numerical results. For model EA, the difference in thickness between the thinnest ice and the thickest ice is only 11 km. Including more elements in the 11 km thick layer and maintaining a reasonable aspect ratio for those elements would require us to increase the horizontal resolution significantly, to a level that is beyond our current computing capacity. However, because model EA has a much smaller mean shell thickness than model GA, so that the EA lateral variations in thickness (which have roughly the same amplitude relative to the mean thickness, as the GA lateral variations) are much smaller than those for GA, we suspect that the 3-D effects from model EA are likely to be even smaller than those from model GA.

### A3. Resolution Test of the Europa Model With (1, 1) Structure in the Icy Shell Shear Modulus

In this section, we perform a resolution test for one of the EC models, where compositionally driven (1, 1) structure with an amplitude of $\delta = 4\%$ is included in the shear modulus of Europa's icy shell. For the 3-D

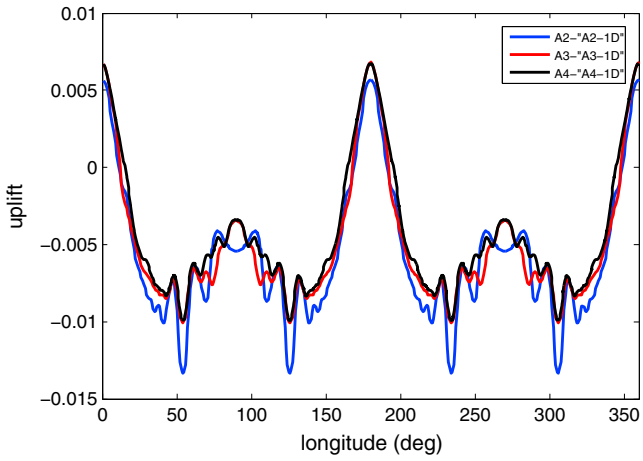


**Figure A3.** Nondimensional surface uplift along the equator of Ganymede. The results are the difference between the 3-D results using model GA and the 1-D results using a shell thickness equal to the mean thickness of model GA (108 km). The normalization used for the uplift results is the same as in Figure 3.


©2014. American Geophysical Union. All Rights Reserved.

**Table A3.** Dominant Spherical Harmonic Coefficients of the Surface Uplift for Europa[a]

| B1–"B1-1D" | | | B2–"B2-1D" | | |
|---|---|---|---|---|---|
| (3, 1) | −1.73E−08 | −2.98E−04 | (3, 1) | −8.94E−09 | −2.99E−04 |
| (1, 1) | −8.23E−09 | −1.29E−04 | (1, 1) | 5.09E−09 | −1.29E−04 |
| (2, 2) | −8.09E−06 | 2.08E−10 | (2, 2) | −8.11E−06 | 4.78E−09 |
| (5, 5) | −4.03E−10 | −3.47E−06 | (5, 5) | 2.89E−09 | −3.47E−06 |
| (5, 3) | −2.87E−09 | 2.95E−06 | (5, 3) | 2.11E−10 | 2.95E−06 |
| (7, 3) | 3.56E−10 | −2.35E−06 | (7, 3) | 2.40E−09 | −2.35E−06 |
| (7, 5) | 1.12E−09 | 1.80E−06 | (7, 5) | −1.17E−09 | 1.81E−06 |
| (13, 3) | −6.68E−09 | −1.31E−06 | (13, 3) | −9.80E−09 | −1.31E−06 |
| (9, 1) | −8.91E−09 | 1.30E−06 | (9, 1) | −4.13E−09 | 1.31E−06 |

[a]The (2, 0) coefficients are not included. The coefficients are the differences between the results for one of the EC models, where compositionally driven (1, 1) structure with an amplitude of $\delta = 4\%$ is included in the shear modulus of the icy shell and the results for a uniform shear modulus in the ice. We use the same normalization as in Table 2.

computations, referred as cases B1 and B2, we use $12 \times 80 \times 80$ elements in the horizontal direction and assign 26 elements in the ocean layer. This grid setup is similar to the highest-resolution setup we use for Ganymede. To resolve the laterally varying shear modulus in the ice, we include 10 and 15 elements in the icy shell for cases B1 and B2, respectively. For the 1-D computations, referred to as cases B1-1D and B2-1D, we use the same grid spacing as for the corresponding 3-D cases. The spherical harmonic coefficients for the surface uplift are shown in Table A3. The results using the two different finite-element grids are nearly identical. In the main text, we use results from case B2.

## A4. Resolution Test of the Ganymede Model With a Partially Grounded Icy Shell

In this section, we compute the surface uplift using model GC1, where the icy shell is partially grounded for longitudes less than 30°. Two grid configurations have been implemented: a low-resolution case, where there are $12 \times 48 \times 48$ elements in the horizontal direction, 5 and 20 elements in the floating icy shell, and the fluid layer, respectively; and a high-resolution case, where we include $12 \times 80 \times 80$ elements in the horizontal direction, 10 and 30 elements in the floating icy shell, and the fluid layer, respectively. The uplift results are shown in Figure A4. There is no high-frequency oscillation in the solutions. Near the ice-ocean interface, where large viscosity contrasts are present, the two results are nearly identical. In the floating part of the icy shell, after improving the resolution, the uplift solution becomes slightly larger than that from the lower resolution case, and this is consistent with the resolution test results using 1-D structures (see Table A1). In general, our two solutions agree with each other very well. In the main text, we use results from the high-resolution case.

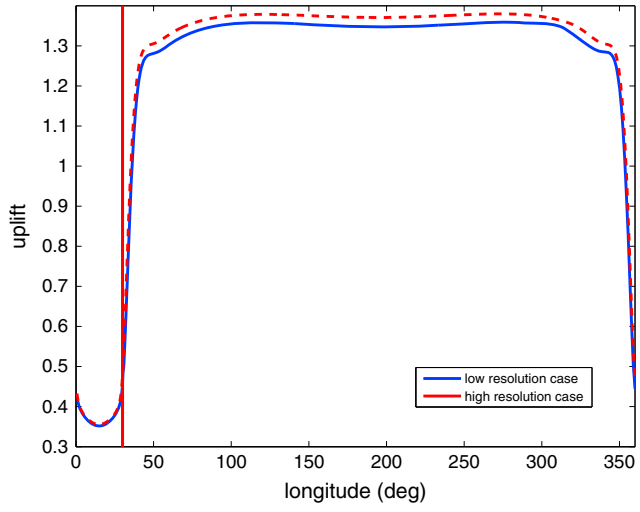


**Figure A4.** Nondimensional surface uplift along the equator of Ganymede for two models with different resolutions. The vertical line shows the grounding line position. The normalization used for the uplift results is the same as in Figure 3.


©2014. American Geophysical Union. All Rights Reserved.

**Acknowledgments**
This work is partially supported by NSF grant NSF-1114168 to the University of Colorado Boulder. We thank Steve Jacobsen and Chuan Qin for helpful discussions. We thank Bert Vermeersen, an anonymous reviewer, and the Associate Editor for their careful reviews.

## References

A, G., J. Wahr, and S. Zhong (2013), Computations of the viscoelastic response of a 3-D compressible Earth to surface loading: An application to Glacial Isostatic Adjustment in Antarctica and Canada, *Geophys. J. Int.*, *192*(2), 557–572, doi:10.1093/gji/ggs030.

Agnew, D. C. (2008), Earth tides, in *Treatise on Geophysics*, Geodesy, vol. 3, edited by T. Herring and G. Schubert, pp. 163–195, Elsevier, Amsterdam.

Alvarellos, J. L., K. J. Zahnle, A. R. Dobrovolskis, and P. Hamill (2008), Transfer of mass from Io to Europa and beyond due to cometary impacts, *Icarus*, *194*(2), 636–646, doi:10.1016/j.icarus.2007.09.025.

Anderson, J. D., E. L. Lau, W. L. Sjogren, G. Schubert, and W. B. Moore (1996), Gravitational constraints on the internal structure of Ganymede, *Nature*, *384*(6609), 541–543, doi:10.1038/384541a0.

Barr, A. C., and A. P. Showman (2009), Heat transfer in Europa's icy shell, in *Europa*, edited by R. T. Pappalardo, W. B. McKinnon, and K. Khurana, pp. 405–430, The University of Arizona Press in collaboration with the Lunar and Planetary Institute, Tucson.

Brown, M. E., and K. P. Hand (2013), Salts and radiation products on the surface of Europa, *Astron. J.*, *145*(4), 110, doi:10.1088/0004-6256/145/4/110. [Available at http://stacks.iop.org/1538-3881/145/i=4/a=110?key=crossref.9426e9d94ea7e7c9a2af07b154bf0f2d.], (Accessed 2 October 2013).

Carlson, R. W., W. M. Calvin, J. B. Dalton, G. B. Hansen, R. L. Hudson, R. E. Johnson, T. B. McCord, and M. H. Moore (2009), Europa's surface composition, in *Europa*, edited by R. T. Pappalardo, W. B. McKinnon, and K. Khurana, pp. 283–327, The University of Arizona Press in collaboration with the Lunar and Planetary Institute, Tucson.

Edmonds, A. R. (1957), *Angular Momentum in Quantum Mechanics*, Princeton Univ. Press, Princeton, N. J.

Edwards, B. C., et al. (1996), The Europa ocean discovery mission, in *Instruments, Methods, and Missions for the Investigation of Extraterrestrial Microorganisms*, Proc. SPIE Int. Soc. Opt. Eng., November, vol. 3111, edited by R. B. Hoover, pp. 249–261, SPIE Press.

Gagnon, R. E., H. Kiefte, M. J. Clouter, and E. Whalley (1988), Pressure dependence of the elastic constants of ice Ih to 2.8 kbar by Brillouin spectroscopy, *J. Chem. Phys.*, *89*(8), 4522, doi:10.1063/1.454792.

Gagnon, R. E., H. Kiefte, M. J. Clouter, and E. Whalley (1990), Acoustic velocities and densities of polycrystalline ice Ih, II, III, V, and VI by Brillouin spectroscopy, *J. Chem. Phys.*, *92*(3), 1909, doi:10.1063/1.458021.

Gammon, P. H., H. Kiefte, M. J. Clouter, and W. W. Denner (1983), Elastic constants of artificial and natural ice samples by Brillouin spectroscopy, *J. Glaciol.*, *29*(103), 433–460.

Jara-Orué, H. M., and B. L. A. Vermeersen (2011), Effects of low-viscous layers and a non-zero obliquity on surface stresses induced by diurnal tides and non-synchronous rotation: The case of Europa, *Icarus*, *215*(1), 417–438, doi:10.1016/j.icarus.2011.05.034.

Kaula, W. M. (1964), Tidal dissipation by solid friction and the resulting orbital evolution, *Rev. Geophys.*, *2*(4), 661–685.

Moore, W., and G. Schubert (2000), The tidal response of Europa, *Icarus*, *147*(1), 317–319, doi:10.1006/icar.2000.6460.

Neumann, G. A., D. D. Rowlands, F. G. Lemoine, D. E. Smith, and M. T. Zuber (2001), Crossover analysis of Mars Orbiter Laser Altimeter data, *J. Geophys. Res.*, *106*(E10), 23,753–23,768, doi:10.1029/2000JE001381.

Nimmo, F., and M. Manga (2009), Geodynamics of Europa's icy shell, in *Europa*, edited by R. T. Pappalardo, W. B. McKinnon, and K. Khurana, pp. 381–404 , The University of Arizona Press in collaboration with the Lunar and Planetary Institute, Tucson.

Nimmo, F., P. Thomas, R. Pappalardo, and W. Moore (2007), The global shape of Europa: Constraints on lateral shell thickness variations, *Icarus*, *191*(1), 183–192, doi:10.1016/j.icarus.2007.04.021.

O'Brien, D., P. Geissler, and R. Greenberg (2002), A melt-through model for chaos formation on Europa, *Icarus*, *156*(1), 152–161, doi:10.1006/icar.2001.6777.

Ojakangas, G. W., and D. J. Stevenson (1989), Thermal state of an ice shell on Europa, *Icarus*, *81*(2), 220–241.

Pappalardo, R. T., et al. (1998), Geological evidence for solid-state convection in Europa's ice shell, *Nature*, *391*(6665), 365–368.

Paulson, A., S. J. Zhong, and J. Wahr (2005), Modeling post-glacial rebound with lateral viscosity variations, *Geophys. J. Int.*, *163*, 357–371.

Qin, C., S. J. Zhong, and J. Wahr (2013), Tidal response of a laterally varying Moon: An application of perturbation theory, 44th Lunar Planet. Sci. Conf., Houston, #2459.

Schubert, G., K. Zhang, M. Kivelson, and J. Anderson (1996), The magnetic field and internal structure of Ganymede, *Nature*, *384*(6609), 544–545, doi:10.1038/384544a0.

Schubert, G., F. Sohl, and H. Hussmann (2009), Interior of Europa, in *Europa*, edited by R. T. Pappalardo, W. B. McKinnon, and K. Khurana, pp. 353–367, The University of Arizona Press in collaboration with the Lunar and Planetary Institute, Tucson.

Smith, E., et al. (2001), Mars Orbiter Laser Altimeter: Experiment summary after the first year of global mapping of Mars, *J. Geophys. Res.*, *106*(E10), 23,689–23,722.

Wahr, J. M., M. T. Zuber, D. E. Smith, and J. I. Lunine (2006), Tides on Europa, and the thickness of Europa's icy shell, *J. Geophys. Res.*, *111*, E12005, doi:10.1029/2006JE002729.

Wahr, J., Z. A. Selvans, M. E. Mullen, A. C. Barr, G. C. Collins, M. M. Selvans, and R. T. Pappalardo (2009), Modeling stresses on satellites due to nonsynchronous rotation and orbital eccentricity using gravitational potential theory, *Icarus*, *200*(1), 188–206, doi:10.1016/j.icarus.2008.11.002.

Wu, X., Y. E. Bar-Sever, W. M. Folkner, J. G. Williams, and J. F. Zumberge (2001), Probing Europa's hidden ocean from tidal effects on orbital dynamics, *Geophys. Res. Lett.*, *28*(11), 2245–2248, doi:10.1029/2000GL012814.

Yoder, C. F., and W. L. Sjogren (1996), Tides on Europa, San Juan Capistrano, California, USA.

Zahnle, K., L. Dones, and H. F. Levison (1998), Cratering rates on the Galilean satellites, *Icarus*, *136*(2), 202–222.

Zahnle, K., P. Schenk, H. Levison, and L. Dones (2003), Cratering rates in the outer solar system, *Icarus*, *163*(2), 263–289, doi:10.1016/S0019-1035(03)00048-4.

Zahnle, K., J. L. Alvarellos, A. Dobrovolskis, and P. Hamill (2008), Secondary and sesquinary craters on Europa, *Icarus*, *194*(2), 660–674, doi:10.1016/j.icarus.2007.10.024.

Zhong, S., A. McNamara, E. Tan, L. Moresi, and M. Gurnis (2008), A benchmark study on mantle convection in a 3-D spherical shell using CitcomS, *Geochem. Geophys. Geosyst.*, *9*, Q10017, doi:10.1029/2008GC002048.

Zhong, S., C. Qin, G. A, and J. Wahr (2012), Can tidal tomography be used to unravel the long-wavelength structure of the lunar interior?, *Geophys. Res. Lett.*, *39*, L15201, doi:10.1029/2012GL052362.

Zhong, S. J., A. Paulson, and J. Wahr (2003), Three-dimensional finite-element modeling of Earth's viscoelastic deformation: Effects of lateral variations in lithospheric thickness, *Geophys. J. Int.*, *155*, 679–695.


©2014. American Geophysical Union. All Rights Reserved.